ELSEVIER

Chemical Engineering Journal 93 (2003) 201–216

Chemical Engineering Journal

www.elsevier.com/locate/cej

Optimization of heat transfer characteristics, flow distribution, and reaction processing for a microstructured reactor/heat-exchanger for optimal performance in platinum catalyzed ammonia oxidation

E.V. Rebrov, S.A. Duinkerke, M.H.J.M. de Croon, J.C. Schouten*

Laboratory of Chemical Reactor Engineering, Schuit Institute of Catalysis, Eindhoven University of Technology, P.O. Box 513, 5600 MB Eindhoven, The Netherlands

Received 14 August 2002; accepted 11 November 2002

Abstract

The present work is focused on the demonstration of the advantages of miniaturized reactor systems which are essential for processes where potential for considerable heat transfer intensification exists as well as for kinetic studies of highly exothermic reactions at near-isothermal conditions. The heat transfer characteristics of four different cross-flow designs of a microstructured reactor/heat-exchanger (MRHE) were studied by CFD simulation using ammonia oxidation on a platinum catalyst as a model reaction. An appropriate distribution of the nitrogen flow used as a coolant can decrease drastically the axial temperature gradient in the reaction channels. In case of a microreactor made of a highly conductive material, the temperature non-uniformity in the reactor is strongly dependent on the distance between the reaction and cooling channels. Appropriate design of a single periodic reactor/heat-exchanger unit, combined with a non-uniform inlet coolant distribution, reduces the temperature gradients in the complete reactor to less than 4 °C, even at conditions corresponding to an adiabatic temperature rise of about 1400 °C, which are generally not accessible in conventional reactors because of the danger of runaway reactions. To obtain the required coolant flow distribution, an optimization study was performed to acquire the particular geometry of the inlet and outlet chambers in the microreactor/heat-exchanger. The predicted temperature profiles are in good agreement with experimental data from temperature sensors located along the reactant and coolant flows. The results demonstrate the clear potential of microstructured devices as reliable instruments for kinetic research as well as for proper heat management in the case of highly exothermic reactions.

Keywords: Microreactor; Heat-exchanger; Ammonia oxidation; Heat transfer

1. Introduction

Process intensification is a novel design approach which aims at reduction of equipment size by several orders of magnitude leading to substantial savings in capital cost, improvement of intrinsic safety, and reduction of environmental impact. Conventional non-adiabatic reactors can be intensified utilizing designs based on compact micro heat-exchangers, where at least one of the streams is replaced by a reacting mixture. Applications for such a reactor can be found in processes where potential for heat transfer intensification exists [1]. Small reactor channel dimensions and high thermal conductivity of the reactor material enable high rates of heat removal [2]. In this way, hot-spot formation and large temperature gradients can be avoided. This is advantageous for a good control of conversion and selectivity of highly exothermic reactions. Furthermore, this technology can be applied to obtain kinetic parameters for kinetically limited reactions. The typical dimensions of microstructured systems are still large enough compared to the mean free path, that classical continuum descriptions can be used. However, the optimization of the thermal behavior of a microstructured metallic reactor is a complicated task, because it is difficult to obtain detailed direct information about the temperature field in the microstructured system. In particular, one wants to avoid undesirable side effects of poor heat-exchange, such as large times required to heat the inlet gas and to quench the outlet mixture, or hot-spots formation and, as a result, overproduction of by-products from competing chemical reactions. Therefore, CFD simulation in combination with a selected number of experiments plays an important role in providing the design of unique microstructured systems of complicated geometry. Recently, Hsing et al. demonstrated that finite element (FEM)

* Corresponding author.
E-mail address: j.c.schouten@tue.nl (J.C. Schouten).
URL: http://www.chem.tue.nl/scr

1385-8947/02/$ – see front matter © 2002 Elsevier Science B.V. All rights reserved.
doi:10.1016/S1385-8947(02)00338-8

Nomenclature

a_1	width of a reaction channel, $a_1 = 1.5 \times 10^{-4}$ m
$\int_A dA = 2.21 \times 10^{-9}$ m^2	the cross-sectional area of the alumina layer (shown in dark gray in (a) and (b) parts of the second figure) in a single reaction channel
b_1	half height of a reaction channel, $b_1 = 5.5 \times 10^{-5}$ m
h	axial coordinate in a cooling channel, $0 < h < 6.5 \times 10^{-3}$ m
i	node number, $1 \leq i \leq 20$
j	reaction channel number, $1 \leq j \leq 20$
k	cooling channel number, $1 \leq k \leq 20$
l	axial coordinate in a reaction channel, $0 < l < 6.5 \times 10^{-3}$ m
n_v	the number of temperature nodes which fall over the reaction channels length, $n_v = 20$
r	radial coordinate in a cooling channel, $0 < r < 1.5 \times 10^{-4}$ m
R	radius of a cooling channel, $R = 1.5 \times 10^{-4}$ m
T_{cat}	catalyst temperature (°C)
$\bar{T}_{cat} = (1/20)\sum_{j=1}^{20} \bar{T}_{cat(j)}$	average catalyst temperature in plane A–A over the set of all reaction channels (°C)
$\bar{T}_{cat(i,j)} = (\int_A T_{cat(i,j)} dA)/\int_A dA$	average catalyst temperature in reaction channel j at the axial position corresponding to temperature node i (°C)
$\bar{T}_{cat(j)} = (1/n_v)\sum_{i=1}^{n_v} \bar{T}_{cat(i,j)}$	average catalyst temperature in reaction channel j (°C)
T_{cold}	coolant temperature (°C)
$\bar{T}_{cold}(h) = (\int_0^R T_{cold} u_{cold} \rho_{cold} r\, dr)/(\int_0^R u_{cold} \rho_{cold} r\, dr)$	average coolant temperature at position h (°C)
T_{gas}	reactant/product gas mixture temperature (°C)
$\bar{T}_{gas}(l) = (\int_0^{b1}\int_0^{a1} T_{gas} u_{gas} \rho_{gas}\, dx\, dy)/(\int_0^{b1}\int_0^{a1} u_{gas} \rho_{gas}\, dx\, dy)$	average reactant/product gas mixture temperature at position l
u_{cold}	coolant velocity (m s^{-1})
$\bar{u}_{cold} = (\int_0^R u_{cold} \rho_{cold} r\, dr)/(\int_0^R \rho_{cold} r\, dr)$	average coolant velocity at position h (m s^{-1})
u_{gas}	velocity of reactant/product gas mixture (m s^{-1})
Greek letters	
ρ_{cold}	coolant density (kg m^{-3})
ρ_{gas}	density of reactant/product gas mixture (kg m^{-3})

simulations could be used as an efficient tool in evaluation of microchemical systems [3]. The feasibility of using a microstructured reactor/heat-exchanger (MRHE) to carry out hydrogen oxidation in a cross-flow arrangement has been experimentally demonstrated by Janicke et al. [4]. In this work, explosive mixtures of gaseous hydrogen and oxygen were safely handled and the hydrogen was completely converted to water on a supported Pt/Al_2O_3 catalyst without explosions.

The present study is a continuation of our previous work [5,6] in which an aluminum microreactor was tested in the ammonia oxidation on a supported Pt catalyst. It was shown that the application of an appropriate design and reactor material could decrease drastically the temperature gradients inside the microreactor even at full conversion of 10 vol.% of ammonia [5]. This result was in agreement with data of Groppi et al. [7] who showed that the thickness of reactor plates and the intrinsic thermal conductivity of the reactor material are the most important parameters to curb effectively the temperature gradients in a highly exothermic reaction. However, in our case a further increase of the ammonia concentration would significantly increase the reactor temperature above the desired value, decreasing the selectivity to the required product, nitrous oxide.

A conventional method for improving the temperature trajectory is to combine a reactor with a heat-exchanger in a co-current or counter-current design of the whole module. In such way, the axial temperature gradient in the reaction channels can be controlled by the temperature and the flow velocity of coolant in the cooling channels [8]. However, in a microreactor of about 1 cm^3 in volume producing about 70 W of heat, up to 50% of the total amount of heat is consumed by heating reactants and coolant. The rest is lost to the environment via reactor housing and fittings [4,9]. Large heat losses to the environment mean that a non-uniform coolant distribution should be applied to withdraw more heat in the center of the MRHE and less near the outer surface of it. The only way to obtain the desired flow

distribution is to construct individual inlet/outlet chambers for each reactor plate that definitely would give rise to heat losses to the environment via the fittings, would complicate the assembling of the MRHE, and finally, would considerably increase production costs. However, in case of a highly conductive reactor material, the "sandwich" cross-flow configuration of a MRHE [10,11] with a non-uniform coolant flow distribution can be effectively used to decrease the axial temperature gradient in the reaction channels as well as to eliminate temperature differences between the different reaction channels to maintain the required accuracy of the kinetic measurements. The temperature field of the MRHE is mainly defined by the diameter and the number of cross-flow cooling channels, the coolant flow rate in the cooling channels, the intrinsic heat conductivity of the reactor material, and the distance between the reaction and cooling channels. Aluminum was chosen as the reactor material because of its high thermal conductivity and ease of micromachining. The effect of the thickness of the aluminum layer between two sets of microchannels on the MRHE performance was explored by comparing the results obtained for each geometry.

The first goal of this work is to enhance the performance of the MRHE by an optimization of the design parameters of a single periodic MRHE unit. An optimized design should provide the possibility to carry out the reaction at near-isothermal conditions at full conversion of 15 vol.% of NH_3, and the possibility to increase the inlet ammonia concentration up to 20 vol.% still without considerable deviations from isothermal behavior. It should be mentioned that the latter case corresponds to an adiabatic temperature rise of about 1800 °C (which more than twice exceeds the aluminum melting point). The goal is to demonstrate that this extreme heat generation can be readily handled in the MRHE. The second goal of this work is to improve the selectivity to nitrous oxide comparing with the microreactor (MR) described in our early work [5], by decreasing the axial temperature gradient in the reaction channels. The axial temperature gradient is caused by the varying reaction and heat production rates along the reaction channels. The idea is to apply a non-uniform flow distribution in the cooling channels with the maximum coolant flow close to the area of maximum heat production. This approach should provide useful information for the future design work on integrated MRHEs for kinetic studies.

Due to large heat losses to the environment, the modeling of a repeated unit, which consists of one reaction channel and one cooling channel, would not be enough to obtain insight on the MRHE behavior. Therefore, three-dimensional (3D) numerical simulation of the MRHE is performed using the FLUENT® code [12]. The results from the reactor modeling, such as gas velocities, gas and material temperatures, and reaction mixture composition, are used as the input data for the performance calculations. Numerical simulations are also performed in order to identify the optimal geometries of the inlet and outlet chambers and the optimal positions of the inlet and outlet pipes in the gas flow distribution system. The design criteria for the reaction channel side were both minimization of the flow non-uniformity, and of the volume of the inlet/outlet chambers to reduce the danger of explosions. The design criterion for the cooling channel side is to obtain a desired flow distribution of coolant. Optimization of the key parameters affecting the temperature distribution in the MRHE is a very complex problem, as these parameters are intricately related and thus cannot be controlled independently. As a first step, we devised an optimization procedure to determine the coolant flow distribution, that results in the most uniform temperature profile at the position of the Pt catalyst. Then an analysis was carried out to find an optimal geometry of the inlet/outlet reactor chambers to obtain the selected coolant distribution. In this way, the performance of several designs was assessed in terms of the differences in flow velocity between the different channels and compared to the optimal flow distribution. It will be shown in this work that appropriate design of the inlet and outlet chambers for reactants and for coolant can be used to feed and withdraw the gases with the desired flow distribution throughout the microchannels.

Finally, we present the experimental data obtained in the MRHE at high ammonia loading. The obtained experimental results support our simulations and show that explosive mixtures of ammonia in oxygen are safely handled and ammonia is completely converted to the reaction products with high nitrous oxide yield.

2. Physical system, computational domain, and reaction kinetics

A schematic view of the MRHE is shown in Fig. 1. The MRHE was designed in order to validate the kinetic model, developed in our previous work [6], in the temperature region below 300 °C with high ammonia inlet concentrations. The heterogeneous Damköhler number (*Da*) representing the ratio of a characteristic heterogeneous reaction rate to a corresponding radial diffusion rate, can be effectively used to determine whether channel dimensions for a given kinetic system are sufficiently small to avoid mass transfer limitations [13]. The diameter of the reaction channels was set at 145 μm. At this diameter, $Da < 0.5$ at all reaction conditions where temperature was below 300 °C. This indicates that the mass transfer in the channels of the microreactor was always greater than the reaction rate, thus diffusion limitations can be neglected. Above 300 °C diffusion limitations were considered by using the CFD FLUENT® code [12]. The length of the reaction channels was fixed at 6.5×10^{-3} m to provide a contact time of 0.33 ms. At this contact time the nitrous oxide yield reaches the maximal value [6]. Estimation of the pressure drop across the reaction channels, according to the expression for an empty tube, gives a difference between the reactor inlet and outlet of about 3.5%. From a practical point of view, it is desirable

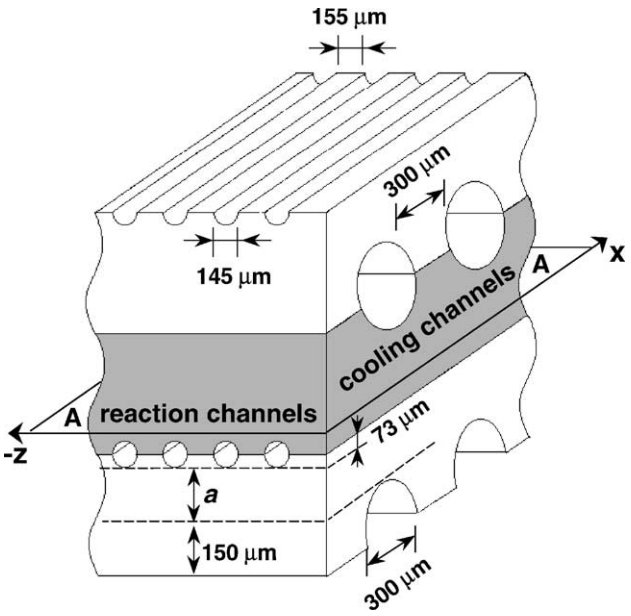

Fig. 1. Schematic view of the microreactor/heat-exchanger: by stacking two plates, a set of reaction channels is produced. By adding a third plate, a set of cooling channels is produced. A single periodic unit, which was the region of numerical simulation, is shown in gray. Plane A–A indicates the position at which the temperature distributions are shown in Fig. 4.

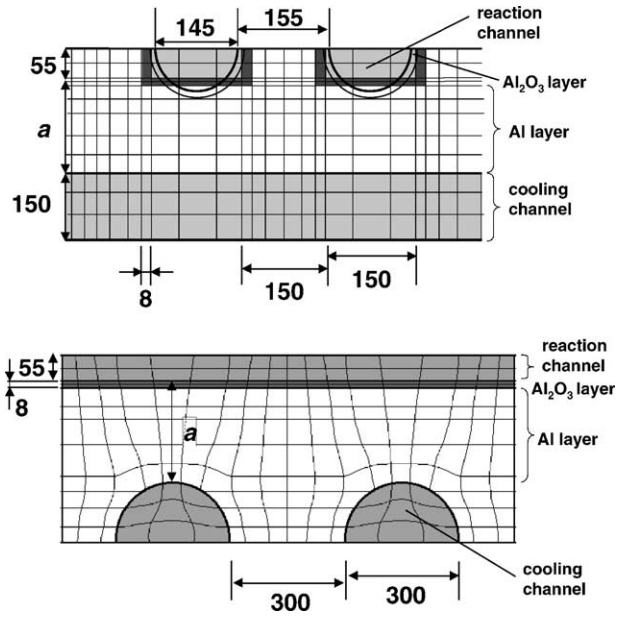

Fig. 2. Comparison between the computational domain and the physical system. A part of the cross-sectional view in the direction of the (a) reaction channels and (b) cooling channels. The shape of the reaction channels was adjusted to the grid lines. The rectangular areas of 150 μm × 55 μm were assigned as a half of the reaction channels. In this way, the cross-sectional area of a whole reaction channel in the computational domain of 1.65×10^{-8} m^2 equals that in the physical system. All dimensions are in micrometers.

that a single microreactor plate has a square shape. Thus, the width of a plate was also fixed at 6.5×10^{-3} m.

The simulation was based on the 3D geometry of a single periodic microreactor/heat-exchanger unit (see Fig. 1). The effect of the thickness of the aluminum layer between two sets of microchannels on the temperature field and the microreactor performance was explored by a separate grid, created for each geometry. To facilitate the grid generation, the shape of the reaction channels in the computational domain was adjusted to the grid lines (Fig. 2). Twenty rectangular areas of 55 μm × 150 μm were assigned as a half of the reaction channels. Four different MRHE designs were studied in which the distance between the reaction and cooling channels (distance *a*, see Figs. 1 and 2) was set at 125, 270, 470, and 670 μm (Table 1). The results obtained on such system will hold as long as there is no significant temperature gradient over the catalyst layer in the direction transverse to the reactant flow. Volume elements next to the reaction channels were assigned as the reaction walls with heat conductivity of the catalyst carrier (alumina), which is equal to 1.0 W m^{-1} K^{-1}. The thickness of these alumina walls was set at 8 μm. The remaining cells between channels were considered as conducting walls with the heat conductivity of aluminum of 230 W m^{-1} K^{-1}. The areas produced by intersecting the planes through the centers of the microchannels were defined as planes of symmetry. The grid validation and solution procedure using the FLUENT® software was reported elsewhere [5]. About 20 h of CPU time (CRAY Origin 2000 supercomputer) were needed for solution convergence. Details of the system geometry and the inlet conditions are given in Table 1.

The cooling system of the MRHE was designed to provide an average temperature of the whole unit at 325 °C at conditions corresponding to an adiabatic temperature rise of 1400 °C. At this temperature the selectivity to nitrous oxide reaches a maximum at a contact time of 0.33 ms [6]. Because a catalyst temperature below 300 °C favors the production of nitrogen [6], the inlet mixture before entering the microreactor reaction mixture has to be preheated in a micromixer to at least 175 °C, in order to avoid an excessive nitrogen production upstream of the microchannels. The heat fluxes in a single reactor plate are listed in Table 2. One can see that at the chosen condition, the reaction produces 6.2 W of heat. A part of this heat is consumed by heating the reaction mixture from the inlet temperature to the reactor temperature. Another part is transferred to the environment. An appropriate value of the heat transfer rate was found based on the data obtained on a similar microreactor with an external surface of 5.0×10^{-4} m^2 containing reaction channels only, which was operated autothermally [5]. At 325 °C this microreactor emitted 80 W to the environment. This corresponds to a heat transfer rate of 1.6×10^5 W m^{-2}. Thus, with increasing the thickness of a single plate from 348 μm (design I) to 893 μm (design IV), the heat losses to the environment rise from 1.2 to 3.5 W. However, for proper comparison the sum of the heat transferred to the environment and to the coolant was kept constant by changing the inlet temperature of the coolant (see Table 2).

Table 1
Parameters of the microreactor/heat-exchanger geometry and inlet conditions

Microreactor/heat-exchanger parameters				
Number of metallic plates in the reactor	8 (+2 top and bottom plates)			
Thickness of the top/bottom plates (mm)	0.6			
Reactor length (mm)	6.5			
Reactor width (mm)	6.5			
Surface area to volume ratio (m^{-1})	6000			
Parameters of a single plate[a]	Reaction channels	Cooling channels		
Number of semi-cylindrical channels per plate	20	9		
Total number of channels in the reactor	100	36		
Channel diameter (μm)	145	300		
Distance between the channels (μm)	155	300		
Cross-sectional area of the channels (mm^2)	1.65	2.55		
Thickness of an alumina layer in channels (μm)	8	–		
Inlet gas composition	NH_3 = 20%; O_2 = 80%	N_2		
Inlet temperature (°C)	175	see Table 2		
Inlet gas flow velocity[b] (STP) ($l\,min^{-1}$)	1.98	5.36		
Inlet gas linear velocity ($m\,s^{-1}$)	20.0	35.0		
Re number (300 °C)	125	450		
Pressure at the channel outlet (atm)	1.0	1.1		
Design parameter and corresponding geometries	Design			
	I	II	III	IV
Distance *a* (μm) (see Fig. 1)	125	270	470	670
Thickness of a single plate (μm)	348	493	693	893
Reactor height (mm)	3.98	5.14	6.74	8.34
Reactor volume (cm^3)	0.168	0.217	0.293	0.352

[a] The parameters are given for a single metal plate having semi-cylindrical channels from each side.
[b] The values are given for the entire module.

To create a non-uniform flow distribution in the cooling channels, it was important to keep the pressure drop below 5% between the coolant inlet and outlet. Higher values of pressure drop implies more resistance to the coolant flow equalizing the flow between different cooling channels. Therefore, the diameter of the cooling channels was set at 300 μm. In this case, nine cooling channels can provide enough cooling capacity when nitrogen gas is used as a coolant. Thus, each element of the MRHE consists of an aluminum plate containing twenty semi-cylindrical reaction channels and nine semi-cylindrical cooling channels machined in perpendicular direction. Each pair of adjacent elements forms a single periodic unit.

Table 2
Heat fluxes in a single reactor plate

Parameters	Design			
	I	II	III	IV
Average ammonia conversion (%)	75			
Heat produced by the reaction (W)	6.2			
Heat consumed by heating the reaction mixture (W)	0.7			
Average reagent/product outlet temperature (°C)	325			
Coolant inlet temperature (°C)	−35	20	105	180
Average coolant outlet temperature (°C)	255	270	295	315
Heat transferred to the coolant (W)	4.3	3.7	2.8	2.0
Heat transferred to the environment (W)	1.2	1.8	2.7	3.5

The ammonia oxidation reaction on the surface of the reaction channels was used as a boundary condition for the chemical species. It should be noted that the kinetic models for ammonia oxidation reported in literature [14–16] are inaccurate at predicting both the activity and selectivities in the microreactor over the temperature interval of interest. The kinetic mechanism for Pt catalyzed ammonia oxidation proposed by Pignet and Schmidt [14], and Hickman and Schmidt [15] predict closed values for turnover frequencies but does not describe the formation of nitrous oxide, which is the major product in our experiments. This is due to the fact that all experiments were performed for reactant pressures between 0.001 and 10 Torr in the 230–1200 °C range, when nitrogen and nitric oxide are the major products. The model of Il'chenko et al. [16] was developed in the 100–250 °C range and being extrapolated to the operating temperature range of the microreactor, overestimates the reaction rate by a factor of 2. Therefore, the kinetic data of the ammonia oxidation on Pt catalyst in a microreactor, obtained in our previous work [5], was used for the present reactor simulations. Catalyst loading was adjusted to 7.5×10^{-3} mol Pt m^{-2} in order to obtain the desired ammonia conversion of 75%. The reaction order with respect to ammonia in the range of NH_3 partial pressures of 0.05–0.20 atm was 0.02, and approached 1.0 at the lowest NH_3 contents. The oxygen

reaction order was −0.06 in the whole range of oxygen partial pressures used in the experiments (0.6–0.8 atm). The detailed mechanism of ammonia oxidation was not used here but an adopted power law form of the rate expression (s^{-1}) was included into the reactor model for temperature profile calculations in the range of 310–340 °C:

$$r_{NH_3} = \frac{k_1 k_2 p_{NH_3}}{(1 + k_1 p_{NH_3}) p_{O_2}^{0.06}} \quad (1)$$

Eq. (1) includes two kinetic parameters with an Arrhenius temperature dependence, $k_1 = k_{10}\, e^{-E_1/RT}$, and $k_2 = k_{20}\, e^{-E_2/RT}$. The strong correlation between the activation energies E_1 and E_2 made it not possible to estimate the individual parameters. The parameter k_1 was fixed at $9.13 \times 10^2\ atm^{-1}$ in the selected temperature range, and the activation energy and pre-exponential factor of k_2 ($72.3\ kJ\ mol^{-1}$, $1.46 \times 10^8\ s^{-1}\ atm^{0.06}$) were found [5]. The constant $N_2/N_2O/NO$ selectivity ratio (47/48/5) obtained in the experiments at 325 °C was used to calculate the heat load in the NH_3 oxidation runs. In spite of the fact that selectivity is a function of temperature, this procedure can be used to evaluate the temperature profile in close vicinity of 325 °C. Indeed, decreasing temperature leads to higher nitrogen selectivity and as a result to a higher rate of the heat production and thus stabilizes the reaction system through a negative feedback between temperature and heat of reaction [6].

3. Microreactor/heat-exchanger simulation

3.1. Simulation responses and objective function

The temperature profiles in the MRHE were calculated at the A–A plane positioned at a distance of 75 μm from the centers of the reaction channels (see Fig. 1). This particular position of the plane for study of the temperature field is chosen, because it is for the most part, within the catalytic Pt/Al_2O_3 layer: the temperature at this position determines the reaction rate of ammonia oxidation. The temperature non-uniformity was determined quantitatively by calculating two responses: the axial (s_1) and transverse (s_2) temperature non-uniformities (see nomenclature for definitions).

The axial non-uniformity was found by averaging the mean-square deviation from the average catalyst temperature in reaction channel j ($\bar{T}_{cat(j)}$), throughout the reaction channels

$$s_1 = \frac{1}{20}\sum_{j=1}^{20}\sqrt{\frac{\sum_{i=1}^{n_v}(\bar{T}_{cat(i,j)} - \bar{T}_{cat(j)})^2}{n_v - 1}} \quad (2)$$

The average catalyst temperature $\bar{T}_{cat(i,j)}$ was taken at 20 positions along the reaction channel j ($n_v = 20$, $1 \le i \le 20$). The nodes were located 300 μm from each other along a reaction channel. The first node was positioned at a distance of 250 μm from the channel inlet.

The temperature non-uniformity in the direction of the cooling channels was found as the mean-square deviation from the average catalyst temperature in plane A–A ($\bar{T}_{cat}$)

$$s_2 = \sqrt{\frac{1}{19}\sum_{j=1}^{20}(\bar{T}_{cat} - \bar{T}_{cat(j)})^2} \quad (3)$$

The goal of the optimization study was to minimize the chosen objective function

$$s = \sqrt{s_1^2 + s_2^2} \quad (4)$$

3.2. Influence of a coolant cross-flow distribution and the aluminum layer thickness

The influence of the coolant flow distribution on the temperature field was studied together with the effect of the aluminum layer thickness to find the optimal design for the MRHE. Temperature profiles at the plane positioned at a distance of 75 μm from the centers of the reaction channels were calculated for designs I–IV (see Table 1) at several different cross-flow distributions of the coolant flow. The coolant flow distributions in the cooling channels are shown in Fig. 3. Results of the simulations are shown in Fig. 4. In case A, simulations were made with the channel cross-sections of all cooling channels exposed to a uniform flow (Fig. 4(a, d, g, j)). In case B, shown in Fig. 4(b, e, h, k), an attempt was made to reduce the temperature non-uniformity by introducing a non-uniform flow distribution in the cooling channels, so the channel with maximal coolant flow is located close to the area of maximal heat production. In this case, the average coolant velocity in cooling channels 1–5 and 6–9 was proportional to the amount of heat evolved in the reaction channels within the corresponding regions of 3.5 and 3.0 mm, respectively (see Fig. 3).

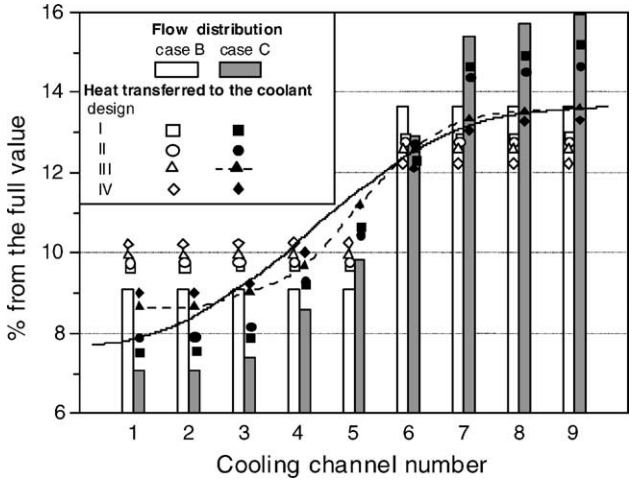

Fig. 3. Coolant flow distributions (vertical bars), heat produced in the reaction channels (solid line), and heat transferred to the coolant for different microreactor designs (symbols). All data are in percent from the full values.

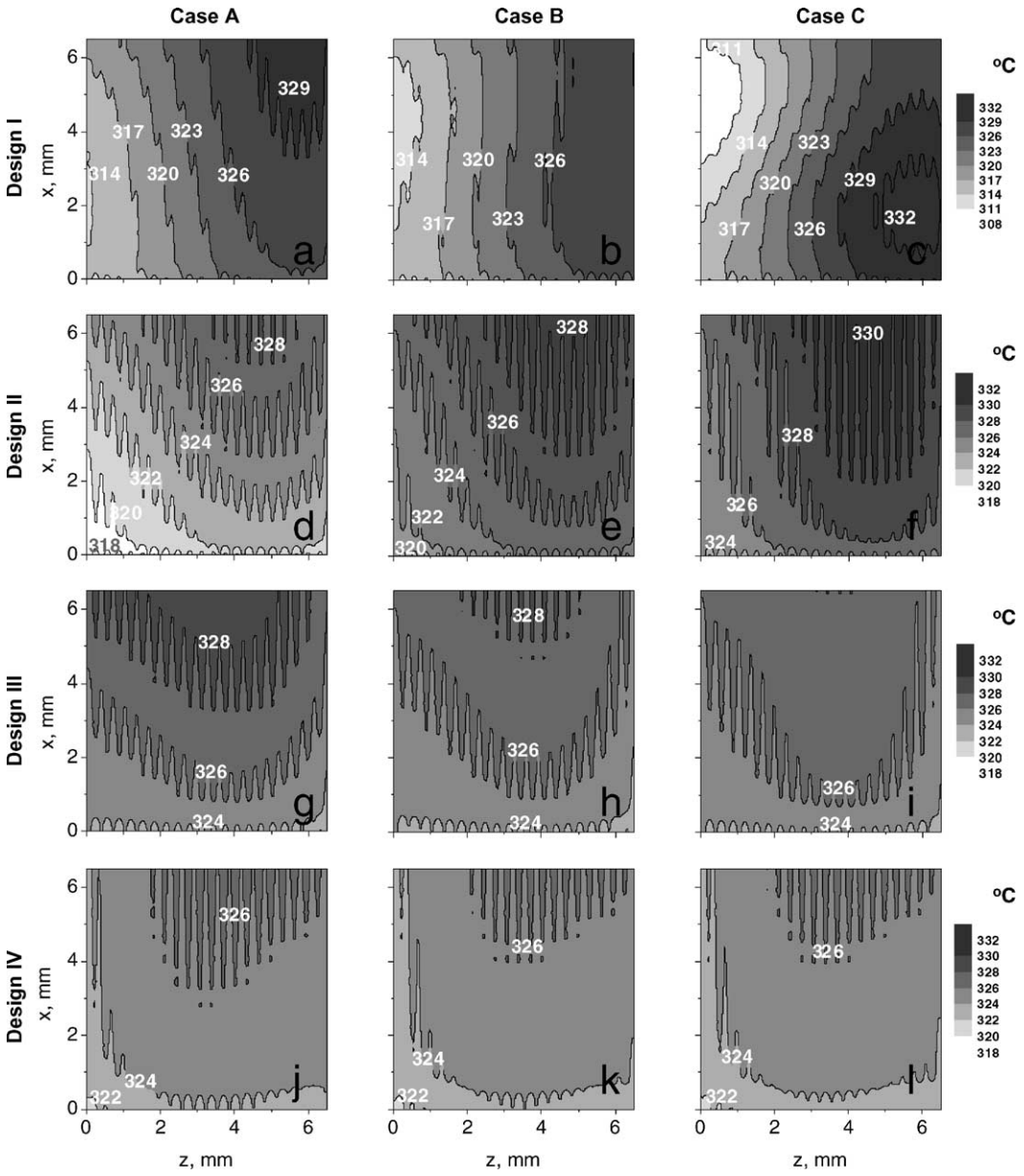

Fig. 4. Temperature distribution at plane A–A. The reagents enters from the bottom, the nitrogen gas enters from the left. Inlet conditions are shown in Tables 1 and 2 (for definitions see Fig. 1).

Table 3
The catalyst temperature non-uniformity in the directions of the reaction channels (s_1) and cooling channels (s_2)

Coolant flow distribution	Design											
	I			II			III			IV		
	s_1	s_2	s	s_1	s_2	s	s_1	s_2	s	s_1	s_2	s
A	1.86	4.92	5.26	2.48	1.59	2.95	1.84	0.51	1.91	1.03	0.48	1.14
B	0.33	5.02	5.03	2.04	1.63	2.61	1.13	0.52	1.24	1.01	0.48	1.12
C	1.67	6.70	6.90	1.75	1.57	2.35	0.89	0.50	1.02	0.98	0.48	1.10

For definition see Section 2.

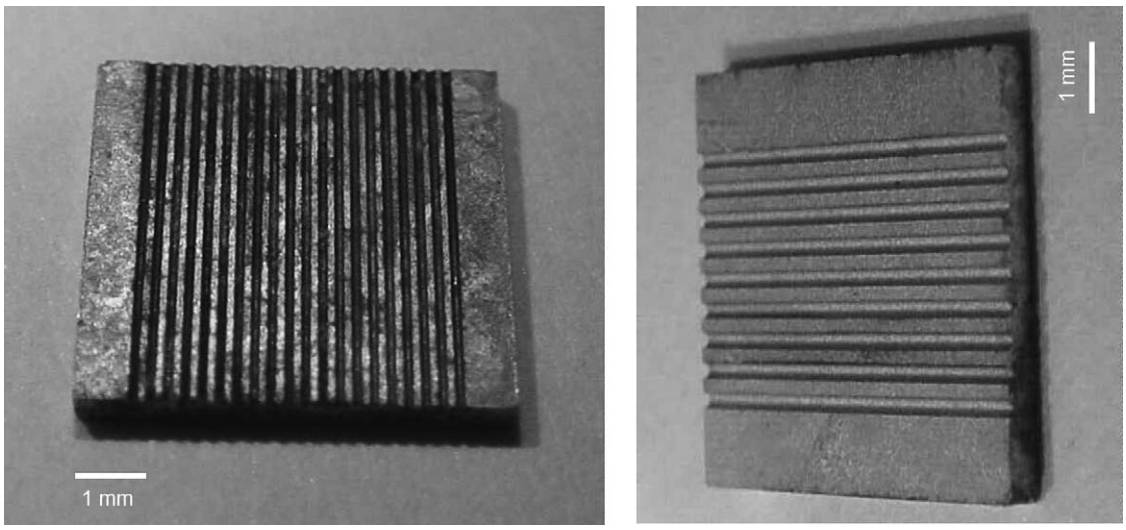

Fig. 5. A single aluminum plate of 6.5 mm × 6.5 mm × 0.693 mm fabricated by the TU/e University workshop according to the optimal reactor/heat-exchanger design. The reaction channel view is shown on the left after impregnation with the Pt catalyst precursor. The black color in the reaction microchannels was due to adsorption of the Pt catalyst precursor. Each plate contains twenty semi-cylindrical reaction microchannels of 145 μm width, 73 μm depth. The cooling channel view is shown on the right. Each plate contains nine cross-flow semi-cylindrical cooling microchannels of 300 μm width, 150 μm depth, arranged at equal distances of 300 μm. The distance between the reaction and cooling channels was 470 μm.

As compared with the uniform flow case A, a considerable reduction by several degrees was observed in the hot-spot temperature in comparison with its initial value, especially for design I. However, increasing the coolant flow velocity by 20% in channels 6–9 in case B provides, in the best case, an increase of the amount of heat transferred to these channels by 15% only, the total amount of heat transferred being the same. Therefore it was decided to apply a substantially more non-uniform coolant distribution. In this way, temperature profiles at several coolant distributions were obtained with the best result observed at the flow distribution which is called case C hereafter (Fig. 4(c, f, i, k)). This flow distribution gave the minimal difference in temperature at the selected position for design III (see Table 3). In case C the average coolant flow velocity in cooling channels 6–9 was 35% higher than in case A (Fig. 4).

The obtained temperature distributions could be explained if it is taken into account that a change in the distance between the reaction and cooling channels produces two effects which act in the opposite way. On the one hand, increasing the distance between two sets of microchannels increases the axial heat conduction through the metal framework, thereby decreasing the temperature gradient and the difference in conversion between 1st and 20th reaction channel. On the other hand, an increased heat conduction in the direction of the reaction channels decreases the positive effect of a non-uniform flow distribution in the cooling channels, thereby increasing the axial temperature gradient along the reaction channels.

Therefore, there is an optimal distance *a* at which the temperature differences in both axial and transverse dimensions are minimal. One can see in Fig. 4(i), that design III combined with the optimal coolant distribution (case C) demonstrates that both axial and transverse temperature gradients across the whole plate do not exceed 3 °C. In this case, the curve of heat transferred to the coolant approaches closely the curve of heat production in the corresponding regions of the reaction channels. Though the results between designs III and IV are practically indistinguishable, increasing the distance between two sets of microchannels increases heat losses to the environment (Table 2) that creates the temperature non-uniformity between the central and outside reaction channels. This effect becomes more pronounced at high distances between the reaction and cooling channels (about 1000 μm) confirming the existence of the optimal distance between two sets of microchannels. However, from the practical point of view, the distance between the reaction and cooling channels has to be set as short as possible to increase the production rate per unit of the reactor volume. Therefore, consideration of any geometry with distance *a* exceeding 670 μm is behind the practical application. Comparing designs III and IV the conclusion can be drawn that any distance *a* in between 470 and 670 μm will not deteriorate the temperature profile substantially.

Using the finalized physical dimensions, the MRHE was constructed (Fig. 5). The actual reactor meets the geometrical design shown in Fig. 1 and Table 1. The fabrication method is discussed in Section 5 in detail.

4. Geometry design of the flow distribution system

A non-uniform flow distribution in the cooling channels considerably improves the temperature field in the MRHE. However, the question remains how to obtain such flow

profile in practice. Modern computational tools for CFD simulations can provide substantial insight into engineering processes involving fluid flows, and can be fruitfully utilized to help improve the design of practical devices. The easiest way to obtain the required flow distribution is to perform CFD simulations on appropriate designs of the inlet/outlet reactor chambers. Recently, Commenge et al. studied the influence of geometrical dimensions of the microstructured reactor on the velocity distribution between channels [17]. For this purpose, an approximate model was developed, based on a simplified description of the reactor as a network of equivalent rectangle ducts. Results calculated with the approximate model were then compared to more detailed finite-volume calculations to validate the approach [18]. The authors proposed to use dimensionless parameters for flow optimization in similar muiltichannel architectures.

A number of alternative designs were chosen to find the best geometry for which the flow distribution gives the minimum difference in temperature at the position of the reaction channels. As attention focused on the gas flow distribution in the cooling and reaction channels, no attempt was made to model the whole MRHE.

4.1. Optimization of inlet/outlet chamber geometry for coolant flow

In the optimization study, the performance of several geometries was assessed in terms of flow distribution and compared to each other. The effect of four design parameters was investigated in the optimization of the chamber geometry (see Fig. 6): the position of the inlet (P1) and outlet (P2) pipes relative to the position of the microchannels, angle a between the chamber wall and the reactor (P3), and distance *d* between the chamber wall and the reactor (P4). Preliminary simulation runs were conducted to determine trends and to establish variable bounds. It was found that the pressure drop required for the desired flow distribution (case C) could not be obtained if the coolant gas is fed or withdrawn near the centerline of the reactor. Therefore, the inlet pipe was fixed near the ninth cooling channel. There proves to be an optimal position for the outlet pipe near the seventh cooling channel at which the trans-chamber pressure drop could provide the desired flow distribution in the cooling microchannels. Furthermore, the chamber width (distance *d*) was fixed at 300 μm to provide conditions at which the desired trans-chamber pressure drop could be obtained. This reduced the number of geometry design parameters to three.

Then, the finite difference method was applied for creating new configurations with separate geometry and grid created for each configuration studied. In this technique, the configuration is systematically modified by shifting the position of the inlet/outlet pipes and angle α through user specified design variables (P1 and P2). The difference between the coolant flow distribution and the reference flow distribution case C (δ_1) was chosen as the objective function

$$\delta_1 = \frac{1}{9}\sum_{k-1}^{9}\left|\bar{u}_{\mathrm{cold}_k} - \bar{u}^*_{\mathrm{cold}_k}\right| \quad (5)$$

where $\bar{u}^*_{\mathrm{cold}_k}$ is the average coolant velocity in channel *k* for the reference flow (case C). The gradient of the objective function with respect to the specified design variables was evaluated. This gradient is used during optimization to calculate a search direction using the steepest descent method. The gradient components are obtained by independently perturbing each design variable with a finite step, calculating the corresponding value of the objective function using CFD analysis, and forming the ratio of the differences. After finding the minimum of the objective function along the search direction, the entire process is repeated until convergence is reached.

Recently, the geometry of the MRHE was laid out using the grid generator PREBFC®, with the geometry specifications imposed by the size of a single periodic unit in design III of the MRHE (Fig. 6). In addition to the inlet/outlet chamber elements, the entrance and exit sections were also modeled as open pipes of a rectangular shape with a height of 1.39 mm and a length of 4 mm. The width of both pipes was fixed at 1 mm to provide a cross-section which is approximately two times larger than the total cross-section in the cooling channels of 0.636 mm^2. For the dimensions shown in Fig. 6, a computational mesh of about 150,000 vol. elements was obtained. The FLUENT® simulation was used to obtain the velocity field. The boundary condition used

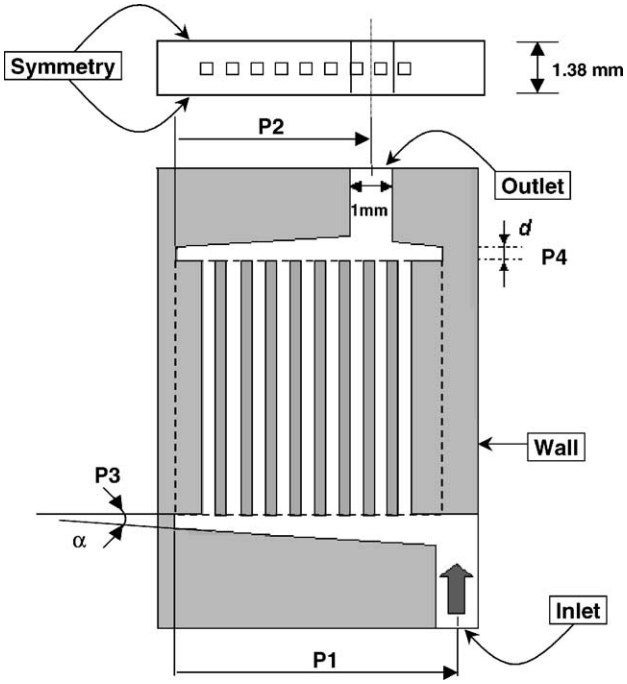

Fig. 6. The design parameters and the dimensions of the inlet and outlet chambers of flow distribution system imposed by the size of a single microreactor plate.

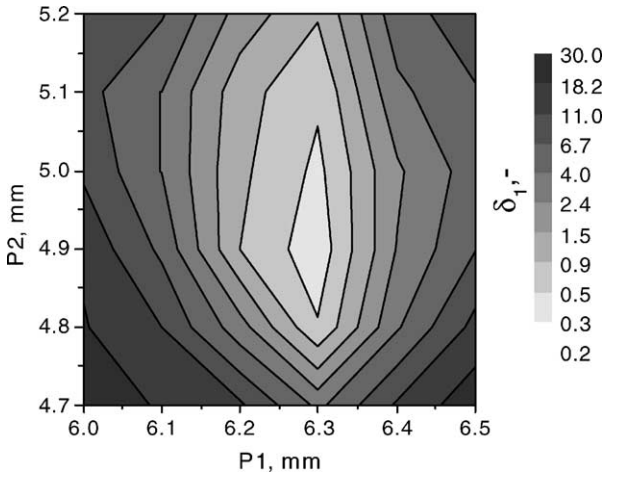

Fig. 7. Dependences of the objective function δ_1 for coolant flow distribution system on the design parameters P1 and P2 (see Fig. 6 for definitions).

at the system inlet was a flat velocity profile in the axial direction. A constant pressure outlet condition was applied.

Fig. 7 demonstrates the mean-square deviation of the coolant flow from the desired flow distribution (case C) as a function of two design parameters: P1 and P2. There is a clear minimum at P1 = 6.3 mm and P2 = 4.9 mm at a constant value of P3 = 5°. It was found that varying P3 in the region 0–10° did not result in any significant change in flow distribution. Fig. 7 shows also that the flow distribution does not change with fluctuations corresponding to the expected physical precision of 25 μm for the positions of the inlet/outlet pipes: both responses fall within 5% from the optimal values.

To control the temperature of the microreactor/heat-exchanger, it is easy to adjust the coolant flow rate than the coolant temperature. Therefore, it is of practical interest what happens with the coolant velocity distribution when the coolant flow changes. Fig. 8 shows that the *Re* number has very little effect on the flow variation from channel to channel. The flow velocity is proportional to the pressure drop between corresponding parts of the inlet and outlet reactor chambers as we showed in [19]. A variation of the *Re* number between 300 and 610 disturbs relative trans-chamber pressure drop and velocity distribution by 6% from the ideal case. This means that in the relatively large range of coolant flows, the same geometry of the inlet/outlet chambers can be applied to obtain the desired coolant distribution.

4.2. Optimization of inlet/outlet chamber geometry for reactant/product flow

The selectivity to the desired product can be further enhanced by creating a uniform residence time distribution in the reaction channels. Furthermore, for research purposes, it is desirable to have uniform flow and fluid properties over the permeation area of the reaction channels.

Similar to the case of optimization of a coolant flow distribution, the performance of several geometries was assessed in terms of reactant flow distribution and compared to each other. Once again, a number of alternative designs were created to find the best geometry. In principle, the generation of a physical grid is the most time consuming procedure in the optimization study. Therefore, to speed up this step, the existing grid for the simulation of the coolant flow was modified using the PREBFC® code to a new grid representing the slab containing 17 reaction channels. For the same reason, to provide a desired total flow through the inlet/outlet chambers, the channel's height and width were set in a modified grid at 150 μm with a distance of 150 μm in between. It should be noted that such geometry does not completely represent the real geometry. However, based on our

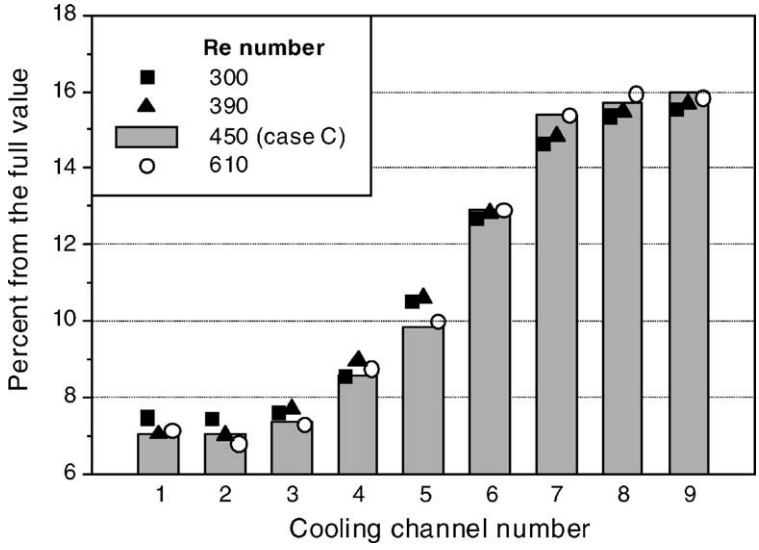

Fig. 8. Flow distribution in the cooling channels as a function of average *Re* number.

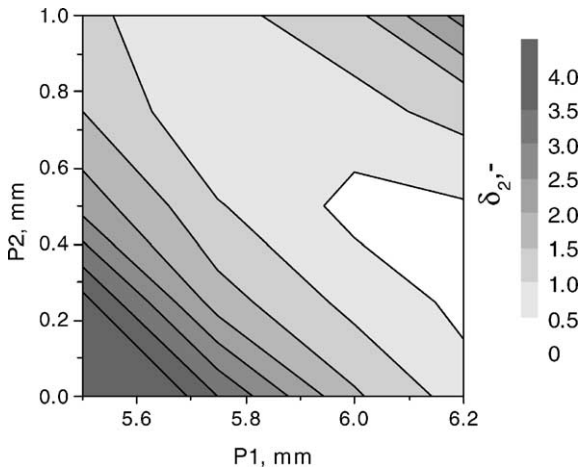

Fig. 9. Dependences of the objective function δ_2 for reactant/product flow distribution system on the design parameters P1 and P2 (see Fig. 6 for definitions).

physical intuition we believe that only minimal differences might exist in the reactant flow profile if we would have used 17 reaction channels instead of 20 of them, because no significant differences were observed for the selected geometry, when the number of channels was increased from 9 to 17. The boundary conditions were chosen the same as those in the case of the coolant flow. The inlet concentrations of 20 and 80 vol.% were applied for ammonia and oxygen, respectively. The change of physical properties of the gas mixture in the course of the reaction was not taken into account. Flow non-uniformity was defined as the normalized standard deviation of the velocity over the permeation area. Parameters P3 and P4 were fixed at 5° and 300 μm, respectively. The mean-square deviation from the average flow velocity was chosen as the objective function

$$\delta_2 = \sqrt{\frac{1}{16}\sum_{j=1}^{17}(\bar{u}_{\text{gas}} - u_{\text{gas}(j)})^2} \quad (6)$$

Fig. 9 shows that δ_2 decreases with increasing P1 and decreasing P2, at a constant value of the sum of these parameters. However, since P1 cannot be increased higher than 6.2 mm due to mechanical restrictions required for proper assembling of the whole module, parameter P2 was fixed at 0.3 mm. One can see in Fig. 9 that the flow distribution does not change with fluctuations corresponding to the physical precision of the system of 25 μm. The CFD simulation of the reactant flow distribution obtained with the selected design parameters.

5. Comparison of CFD simulation and experiment

Ammonia oxidation on a Pt catalyst serves as a good test reaction to evaluate the temperature field in the MRHE. The selectivity toward nitrous oxide has a sharp maximum at about 325 °C [5,6]. Therefore, the highest possible N_2O yield can only be obtained in the reactor operating at isothermal conditions. In order to validate experimentally the behavior of the MRHE, the reactor was constructed in the TU/e University workshop according to the developed design. The reactor consists of eight aluminum plates of 6.5 mm × 6.5 mm, each of them containing twenty semi-cylindrical reaction microchannels of 145 μm width, 73 μm depth, arranged at equal distances of 155 μm from one side, and nine cross-flow semi-cylindrical cooling microchannels of 300 μm width, 150 μm depth, arranged at equal distances of 300 μm from the opposite side of the plate. The top and bottom plates contain reaction semi-channels only. The microchannels were produced by electric discharge machining [20]. This method is commonly referred to as spark erosion because it machines two electrically conductive materials using electrical discharges, or sparks. During this process, a spark is generated from an electrode to a work piece. With each electric discharge, a minute metal particle is eroded from the work piece at the location of the smallest gap between the two objects. This process occurs up to 2.5×10^5 Hz, and takes place with the work piece submerged in a liquid dielectric medium. The liquid serves as a flushing agent for the metal particles as well as an insulator and coolant. The absence of heat and pressure is the ideal environment for producing the most precise metal-to-metal relationship attainable by any method of machining available today.

To create a high surface area alumina which was used as carrier for the Pt catalyst, each aluminum plate was exposed to anodic oxidation in a 10 wt.% oxalic acid solution for 1 h at 18 °C. This procedure was similar to that used by Wießmeier and Hönicke [21]. These authors kept the constant voltage by using a special power supply unit. In our study, the current density was kept constant at 15 mA cm^{-2} by changing the applied voltage in the range of 45–55 V. At applied conditions, an 8 μm alumina layer was produced. Before reactor assembly and catalyst impregnation, the aluminum plates were polished to remove the oxide layer between the channels. The weight of the alumina layer in the reaction channels was 1.95 mg for the complete reactor. Platinum impregnation was done with a 1:1 molar solution of chloroplatinic and citric acids, which was circulated through the reaction channels at room temperature for 6 h. To obtain an even Pt distribution throughout the total length of the channel, the flow direction was altered every 30 min. After the impregnation, the plates were heated at 2 °C min^{-1} to 450 °C in oxygen flow and held at this temperature for 6 h.

To quantitatively determine the total amount of Pt and to estimate the average Pt particle size in the microchannels, a test plate containing the reaction channels only was used. According to XPS data, the atomic Pt/Al ratio was 0.71. Prior to the kinetic experiments, the catalyst was reduced in a 10% hydrogen in He flow at 340 °C. The low reduction rate is favorable to obtain high Pt dispersion. The reduction of PtO on alumina with hydrogen starts at 310 °C and proceeds easily at the chosen temperature. According to the

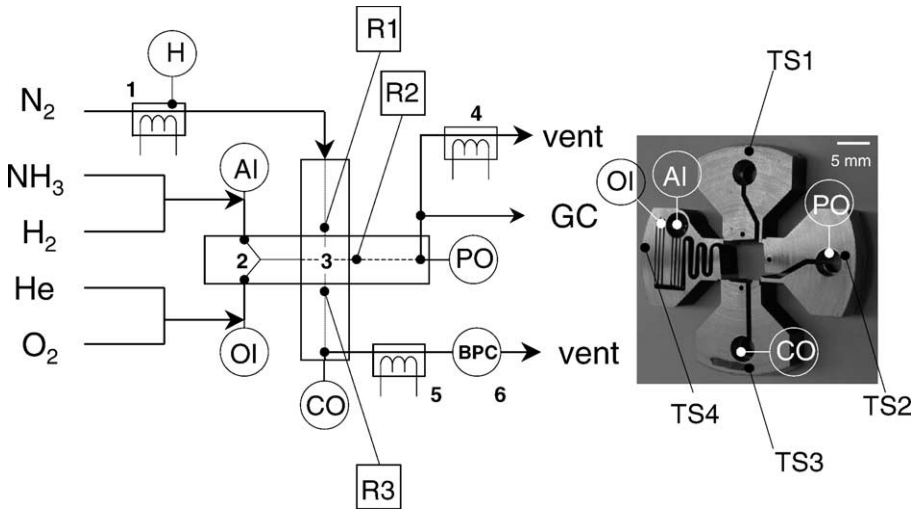

Fig. 10. Flow chart (on the left) and the detailed view of the optimized configuration of the inlet/outlet chambers for the reagents/products and the coolant (on the right). Definitions: (1) external heater; (2) micromixer combined with the inlet reagent chamber; (3) microreactor/heat-exchanger chamber (the reactor not inserted); (4) cold trap; (5) second heat-exchanger (to protect the back pressure controller from the hot nitrogen flow); (6) back pressure controller. Thermocouples: H, external heater; AI, ammonia inlet; OI, oxygen inlet; PO, product outlet; CO, coolant outlet; R1, R2, R3, temperature inside reactor's chambers at the distance of 1 mm from the corresponding reactor walls; S0, S1, S2, S3, temperature on the outer surface of the corresponding chambers of the microreactor/heat-exchanger; S0, reagent inlet; S1, R1, coolant inlet; S2, R2, product outlet; S3, R3, coolant outlet.

XPS data complete reduction was observed after 6 h. The average Pt particle size based on hydrogen chemisorption data was 4.5 nm. This corresponds to a Pt dispersion of 20%.

The complete flow chart of the experimental set-up is shown in Fig. 10. To provide an effective mixing and preheating the reaction mixture to the desired temperature, a micromixer combined with the inlet chamber was positioned upstream of the MRHE. The micromixer consists of two inlets for the reactants, a channel to mix the gases, and the outlet to the reactant chamber. The external heater was inserted in the N_2 line to initiate the reaction. The reaction was started by passing 5 l min^{-1} of preheated N_2 through the cooling channels and 0.5 l min^{-1} of 20% H_2, 10% NH_3, 20% O_2 mixture in He. The N_2 heater was operated by a PID controller with the reactor temperature (thermocouple R2) as a response. The hydrogen oxidation reaction started at about 90 °C, assisting in raising the reactor temperature rapidly to the final operating temperature. At the temperature of about 270 °C, the hydrogen flow was gradually switched off and the ammonia and oxygen flows were adjusted to the desired values. It should be mentioned that more than 30 h (four experimental runs of 4–12 h) were necessary to reach reproducible data. This is due to the well-known effect of the reconstruction of a Pt surface under experimental conditions [22,23]. A considerable improvement in the induction period was also observed with each successive experimental run. This is in accordance with the early published results obtained by Janicke et al. who observed a decrease in the induction period for hydrogen oxidation on a Pt catalyst from over 90 min to approximately 5 min after five experimental runs [4,9]. After leaving the reactor, approximately 0.1% of the total outlet flow was sent to the GC. The main flow was directed to a cold trap maintained at 2 °C which was used to remove water from the exit flow. A heat-exchanger was also inserted in the coolant line to protect the back pressure controller from the hot nitrogen flow. The back pressure controller was used to keep the coolant pressure slightly above the reactant pressure to prevent a risk of possible reactant leakage to the coolant line. However, in the absence of catalytic reaction, the nitrogen background in the He flow did not exceed 10 ppm at all measured temperatures.

Fig. 11 shows the temperature at different positions in the MRHE as a function of time. After heating the nitrogen flow, the temperature of the MRHE increased. After 3 min time, the hydrogen oxidation reaction ignited and additionally heated the product flow. As this happened, the temperature at position R2 was always higher than that at position R3. After 12 min, the temperature reached the set-point and the heater was switched off. After adjustment of the flow velocities of ammonia, oxygen and nitrogen, the targeted steady-state was reached. At these steady-state conditions, the temperature at the product outlet side (R2) was 2 °C higher than that at the coolant outlet side (R3). In turn, the temperature at the coolant outlet side (R3) was 2 °C higher than that at the coolant inlet side (R1). The temperature of the product mixture at a position 12 mm downstream of the reactor outlet was 297 °C (PO), which is 25 °C lower than that at the reactor channel outlet. The temperature of the coolant flow at a position 12 mm downstream of the reactor was 277 °C (CO), which is about 20 °C lower than that of the product flow. Such differences can be explained, if the temperature of the coolant flow at the outlet of the cooling channels does not reach the temperature of the reactor wall. Otherwise, the gas temperature at the position of the coolant outlet port (CO) should be higher than the temperature at the position of the product outlet port (PO), because

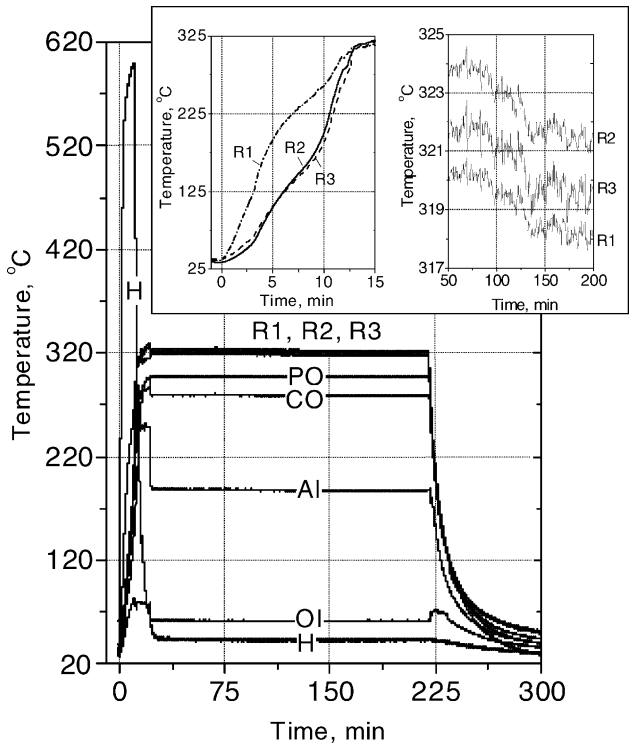

Fig. 11. Temperature responses for the microreactor/heat-exchanger (for definitions see Fig. 10). Reagent flow rate at steady-state conditions: NH_3 0.30 l min^{-1}, oxygen 1.70 l min^{-1}, coolant 5.36 l min^{-1}. In the frame on the left side a detailed view of the start-up interval is shown. After 3 min time, the hydrogen oxidation reaction ignited, as temperature R2 was higher than temperature R3 for the rest of the experiment. After the heater was switched off, temperature R3 was always higher than temperature R1. This is clearly shown in the frame on the right side. After ammonia supply was switched off, the reaction was quenched immediately and it took 3 min to decrease the temperature below 200 °C.

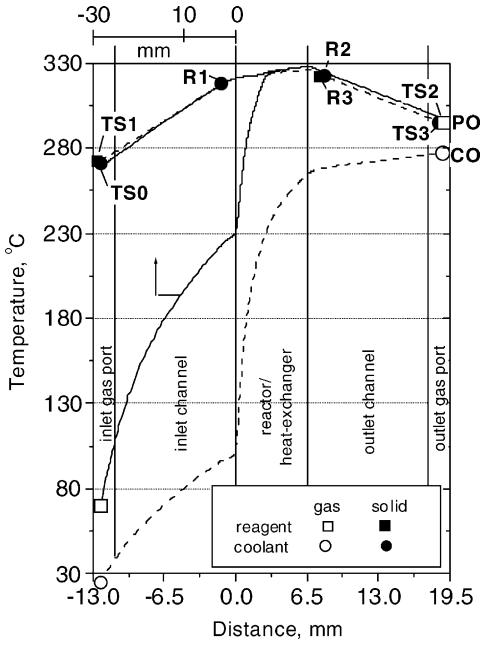

Fig. 12. Temperature of solid material and gas flow along the gas flow pathway. Experimentally measured temperatures (symbols) vs. fluent simulation (lines). Closed symbols are given for the temperature of channel walls, open symbols are given for the average temperature of appropriate gas flows. Solid lines are given for reagents/product mixture, dashed lines are given for the coolant. Inlet conditions are the same as those in Fig. 11.

the flow velocity of nitrogen flow is about 2.5 times larger than that of the product flow. This result is confirmed by CFD simulations which gave the coolant outlet flow temperature of 295 °C at the inlet temperature of 105 °C (see Tables 1 and 2). However, in the actual experiment, the nitrogen flow entering the inlet port at a temperature of 25 °C (see Figs. 11 and 12) was heated up to 100 °C at the position of the cooling channel inlet. This estimation is based on the temperature gradient of 3.9 °C mm^{-1} for the wall of the channel connecting the nitrogen inlet port being at 273 °C (S1), with the coolant inlet chamber (R1). Therefore, nitrogen enters the inlet coolant chamber at 100 °C, leaving the outlet coolant chamber at 268 °C, warming up to 277 °C in the outlet channel connecting the outlet chamber with the outlet coolant port (S3). The same estimation made for the reactant flow leads to the conclusion that reactants enter the reaction channels at 225 °C, leaving them at 325 °C, finally cooling down to 295 °C (PO) in the outlet channel. The fact that the temperature of the coolant flow at the outlet from the cooling channels is still somewhat below the wall temperature, is also confirmed by the difference of 2 °C in temperature between positions R1 and R2.

To make a complete analysis of the heat balances in the MRHE, we also have to know the selectivities to all reaction products. Fig. 13 shows nitrogen, nitrous oxide, and nitric oxide selectivity as a function of the O_2/NH_3 molar ratio. Temperature R2 was 323 °C and the total flow velocity was

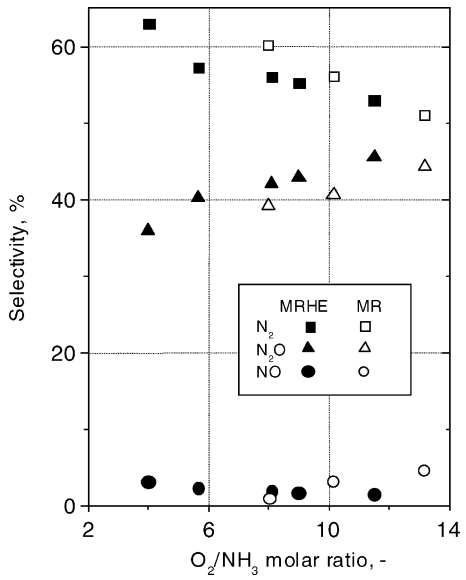

Fig. 13. Selectivity to nitrogen, nitrous oxide, and nitric oxide as a function of O_2/NH_3 ratio. Temperatures R1, 319 °C; R2, 323 °C; R3, 321 °C. Total flow rate in the reaction channels: 2.04 l min^{-1}. No diluent gas was used in all experiments.

Table 4
Simulated vs. experimental heat fluxes in the microreactor/heat-exchanger

Parameters	CFD	Experimental
Reagent inlet flow (STP) ($l\,min^{-1}$)	1.98	2.00
Coolant inlet flow (STP) ($l\,min^{-1}$)	5.36	5.40
Ammonia inlet concentration (%)	20.0	15.0
Oxygen inlet concentration (%)	80.0	85.0
Average ammonia conversion (%)	75	100
Selectivity to N_2 (%)	47	58
Selectivity to N_2O (%)	48	40
Selectivity to NO (%)	5	2
Coolant inlet temperature (°C)	105	100[a]
Average coolant outlet temperature (°C)	295	268[a]
Reagent inlet temperature (°C)	175	225[a]
Average reagent/product outlet temperature (°C)	325	325
Heat produced by the reaction (W)	62	67
Heat consumed by heating the reaction mixture (W)	7	6
Heat transferred to the coolant (W)	28	25
Heat transferred to the environment (W)	27	36

[a] Not measured directly. Estimation is based on the result of appropriate FEM simulations (see Fig. 12).

$2.0\,l\,min^{-1}$ in all experiments. The nitrogen flow was adjusted to maintain the desired temperature. At full conversion of 15% NH_3 in oxygen ($O_2/NH_3 = 5.7$), the selectivity ratio ($N_2/N_2O/NO$) of 58/40/2 was obtained. It should be mentioned that as the NH_3/O_2 ratio increases, the selectivity to N_2O decreases. Therefore the result obtained in the MRHE is in general agreement with the previously developed kinetic model [6]. However, a detailed kinetic analysis for ammonia oxidation with high ammonia inlet concentrations is definitely out of the scope of this publication. Table 4 compares heat balances based on the CFD simulation with the experiment. A rather good agreement is obtained between the simulation results and the experimental data. Furthermore, approximately half of the 67 W of heat produced by the reaction is used to heat the reactant and coolant gases. Almost the same amount is transported to the environment via the outer surface of the MRHE. The latter is not measured directly, but is obtained by an energy balance over the system.

The total amount of water produced in the experiment was also measured. In one such experiment, 83 g of water was produced during 4 h, corresponding to a rate of $0.35\,g\,min^{-1}$. From the ammonia flow rate of $0.3\,l\,min^{-1}$, assuming ideal gas behavior and taking into account the amount of the uncondensed water and water in the GC flow, the rate at which water would be produced is $0.35\,g\,min^{-1}$. The amount of uncondensed water in the gases exiting the condenser was calculated based on a water vapor partial pressure of 0.7 kPa at a gas exit temperature of 2 °C [24]. Thus, a very good agreement between the ammonia consumption rate and the rate of water production is observed.

An additional number of experiments were carried out to compare the behavior of the MRHE and a microstructured reactor without a heat-exchanger (MR) used in [6] to study ammonia oxidation kinetics. The latter consists of seven sets of cylindrical channels. Each set contains seven channels of 280 μm in diameter, 9 mm long. The basic material for this reactor was also aluminum. It was estimated that a temperature gradient as large as 14 °C existed along the axial direction at full conversion of 6.6% ammonia in oxygen mixture. This led to extensive nitrogen production upstream of the microchannels decreasing the overall selectivity to nitrous oxide. Fig. 13 clearly shows that the MRHE yields more N_2O than the MR in the whole range of conditions studied. This is definitely due to the very flat temperature profile in the MRHE.

To test the effect of higher reactant flow rates and higher ammonia inlet partial pressures, a set of experiments with higher ammonia inlet concentrations and reactant flow velocities was carried out. The results are summarized in Table 5. With the results presented, it is clear that the average operating temperature can be still maintained at the desired value through the compositions and flow rates of the reactant gas mixture and the coolant. However, a moderate deviation from isothermal condition was observed at power loadings exceeding the design value of 62 W. As a result, the overall selectivity to nitrous oxide was moderately lower than that expected at isothermal conditions according to the kinetic model [6].

Table 5
Heat management in the microreactor/heat-exchanger at different ammonia inlet concentrations and reagent flow velocities

Parameters	Ammonia inlet concentrations				Reagent flow velocities			
Reagent inlet flow (STP) ($l\,min^{-1}$)	2.00	2.10	2.03	2.12	2.00	2.20	2.40	2.70
Coolant inlet flow (STP) ($l\,min^{-1}$)	5.40	10.4	11.3	12.5	5.40	6.12	6.85	9.95
Ammonia inlet concentration[a] (%)	15.0	20.0	21.3	22.8	15.0	15.3	15.3	15.3
Heat produced by the reaction[b] (W)	67	94	98	105	67	74	81	91
Selectivity to N_2 (%)	58	63	63	65	58	61	63	64
Selectivity to N_2O (%)	40	34	33	30	40	37	34	33
Selectivity to NO (%)	2	3	4	5	2	2	3	3
Temperature R1 (°C)	321	311	309	307	321	315	310	304
Temperature R2 (°C)	325	325	325	325	325	325	325	325
Temperature R3 (°C)	323	320	319	318	323	323	323	323
ΔT_{max} (°C)	4	14	16	18	4	10	15	19

[a] Oxygen was the balance in all experiments.
[b] Ammonia was fully converted to the reaction products in all experiments.

6. Discussion

Because the CFD was followed by the experiment, it was difficult to predict in the beginning the Pt dispersion (hence the reaction rate) and the amount of heat released to the environment. We fixed the reactant and coolant flow velocities as well as their inlet and outlet temperatures to their values in the CFD model. In fact using a low reduction temperature we obtained a more active catalyst than that we previously described [5] after reduction at 400 °C. Because the experiment was done to validate CFD calculations it had to be performed at a similar value of the adiabatic temperature rise. Therefore, we had to decrease the ammonia inlet concentration (fitted parameter) to 15% in the experiment. Furthermore, as it can be seen from Table 5, the amount of heat released to the environment, mainly via reactor connections, was underestimated by 30% in the CFD model.

It is interesting to compare the results obtained in this study with early published literature data. Drost et al. developed a MRHE that heats water using methane combustion. The authors studied this MRHE over a range of reactant partial pressures and gas and water flow rates. Heat transfer rates between 8.5 and 21 W cm^{-2} were achieved in the MRHE [25,26]. In our MRHE, a heat transfer rate as high as 85 W cm^{-2} was observed between two gaseous flows, which four times exceeds the maximum value reported in [25]. The heat flux was calculated based on the amount of heat transferred to the coolant per unit interface area in the cooling channels. In fact, with a cross-flow design, a thermal power generation and transfer of more than 400 W in a cubic centimeter seems to be possible without considerable deviation from isothermal conditions in the solid material. Another interesting result is that the reaction gas exits the reactor at the temperature of the catalytic wall, while the coolant exits at a temperature which is below or equal to the temperature of the solid material. This result, which was also predicted by CFD simulations, is in sharp contrast with the data obtained by Janicke et al., where the temperature of the N_2 cooling gas was always higher than the temperature of the reaction gases [4]. These authors studied the Pt catalyzed hydrogen oxidation in a cross-flow MRHE. They explained such result by formation of a hot-spot in the front zone of the reaction channels and subsequent cooling of the reactant gases downstream of the reaction microchannels [4]. It should be mentioned, that the MRHE, used in their work, was assembled from individual stainless steel plates, which were coated with alumina. The intrinsic thermal conductivity of stainless steel is approximately 15 times less than that of aluminum. Therefore, heat produced mainly in the front zone of the reaction channels cannot be transferred effectively downstream of the microchannels, and thus creates a considerable temperature gradient. This effect was even more pronounced when a heat transfer oil was used instead of nitrogen as coolant [9]. In such an experiment, the outlet temperature of the oil was more than 130 °C higher than that of the product gas. In their experiment, the exit temperature of the oil was the average of hot oil at 270 °C near the reaction channel entrance and colder oil at 70 °C near the exit. Such a temperature gradient in the reaction channels can maximize the yield of products of a reversible exothermic reaction [8]. However, it deteriorates the yield of a partial oxidation product, which has a sharp maximum in selectivity at a definite temperature. Maintaining the operating temperature between 35 and 75 °C, Görke et al. investigated the intrinsic reaction kinetics of the platinum catalyzed hydrogen oxidation in a stainless steel based MRHE, operating in the differential mode at near-isothermal conditions [27]. Note, that in this MRHE the ratio of Pt-coated steel foils in the reaction passage to the perpendicular water-carrying steel foils of the same geometry was 1:3. In this case, the highest temperature difference of 2 °C was observed between the inlet and outlet positions at a maximum reaction power of 35 W. The preheated water with a temperature just a little below the reactor temperature was pumped with a flow of 250 g min^{-1} through the cooling channels. The volume of this MRHE of 0.314 cm^3 is close to the volume of the MRHE designed in the present study (see Table 1). However, it produces two times less power in the low temperature range, i.e. at temperatures near the temperature of the environment. One can see from the above-mentioned examples that an increase of the operating temperature, or a transition to the integral mode of operation would increase drastically the temperature gradient in the reaction channels. Therefore, such a system can be used for studying only a very limited number of catalytic reactions.

These examples demonstrate clearly that the choice of basic material plays a crucial role in managing the temperature profile of a MRHE. An aluminum microreactor has a maximum operating temperature at about 400 °C, while numerous catalytic applications require temperatures higher than this. In order to realize such applications, new techniques must be developed for producing microchannels in refractory metals, or aluminide intermetallics. These materials have high melting points, a good corrosion resistance and a relatively low thermal expansion coefficient. Some of them have also a rather high thermal conductivity, which is, however, a factor 2–4 less than that of aluminum. The corrosion resistance of most of these materials can be improved by electrochemical deposition of thin niobium or hafnium films [28].

In our study we assumed microchannels have no distribution of neither channel diameter nor catalyst coating thickness. However, both these parameters have dispersion in the actual MRHE that certainly has an impact on the temperature profile and flow distribution. We tried to diminish such uncertainties by a proper choice of techniques applied. In this way, anodic oxidation in an oxalic acid solution was chosen to produce an alumina layer, because this method produces rather uniform coatings with relative difference in thickness of about 5%. At the same time, electric discharge machining gives better mechanical precision as compared with either micro milling with shaped diamond tools or laser ablation techniques. It is not the aim of this paper to evaluate

the influence of the channel diameter non-uniformity, but a further decrease in channel diameter below 100 μm would require to investigate these effects.

From the above, it will be clear that, MRHE made of highly conductive materials can be used as an efficient tool for the determination of intrinsic kinetics of fast, strongly exothermic catalytic reactions at near-isothermal conditions both in the differential and integral modes. Sufficiently small temperature gradients, as observed in these systems, considerably simplify the extraction of kinetic parameters from experimental data.

7. Conclusion

An appropriate design of a single microstructured plate decreased the temperature non-uniformity in the complete reactor to less than 4 °C even at conditions corresponding to an adiabatic increase of temperature of about 1400 °C. In case of a microreactor made of a highly conductive material (i.e. aluminum), there is an optimal distance between the reaction and cooling channels in the single microstructured plate. Optimizing the heat conduction throughout the metal framework by changing the distance between the reaction and cooling channels, the temperature non-uniformity between the outside reaction channels can be decreased to about 2 °C, providing virtually the same degree of reactant conversion and product selectivity. Furthermore, a non-uniform coolant distribution decreases the axial temperature gradient in the reaction channels to less than 3 °C. The experiments with the microreactor/heat-exchanger clearly demonstrates that the selectivity to a partial oxidation product can be considerably improved by conducting the catalytic reaction at near-isothermal conditions. Furthermore, the good agreement between simulated and observed results demonstrates the ability of CFD simulations to predict accurately the behavior of a MRHE. In this way, a MRHE can provide a high level of accuracy in a kinetic study of strongly exothermic catalytic reaction. Further research with this microreactor/heat-exchanger system will continue to validate the kinetic scheme for ammonia oxidation reaction at even higher ammonia loadings.

Acknowledgements

The authors would like to thank Theo Maas, Erwin Dekkers, and Jurgen Bulsink from the TU/e University workshop for their work on the construction of the microstructured reactor/heat-exchanger.

References

[1] A. Green, Chem. Ind. London 5 (1998) 168.
[2] W. Ehrfeld, V. Hessel, H. Möbius, Th. Richter, K. Russow, in: Dechema Monographs, Potentials and Realization of Microreactors, vol. 132, Verlag Chemie Weinheim, Verlagsgesellschaft, 1996, p. 1.
[3] I.M. Hsing, R. Srinivasan, M.P. Harold, K.F. Jensen, M.A. Schmidt, Chem. Eng. Sci. 55 (2000) 3.
[4] M. Janicke, H. Kestenbaum, U. Hagendorf, F. Schüth, M. Fichtner, K. Schubert, J. Catal. 191 (2000) 282.
[5] E.V. Rebrov, M.H.J.M. de Croon, J.C. Schouten, Catal. Today 69 (2001) 183.
[6] E.V. Rebrov, M.H.J.M. de Croon, J.C. Schouten, Development of the kinetic model of platinum catalyzed ammonia oxidation in a microreactor, Chem. Eng. J. 90 (2002) 61.
[7] G. Groppi, G. Airoldi, C. Cristiani, E. Tronconi, Catal. Today 60 (2000) 57.
[8] W.E. TeGrotenhuis, D.L. King, K.P. Brooks, B.J. Golladay, R.S. Wegeng, Optimization of microchannel reactors by trading-off equilibrium and reaction kinetics througth temperature management, in: Proceedings of the 6th International Conference on Microreaction Technology, New Orleans, LA, USA, 2002, p. 18.
[9] M. Janicke, A. Holzwarth, M. Fichtner, K. Schubert, F. Schüth, Stud. Surf. Sci. Catal. 130 (2000) 437.
[10] E.V. Rebrov, M.H.J.M. de Croon, J.C. Schouten, Chem. Ingenieur Tech. 73 (2001) 676.
[11] A. Wenka, M. Fichtner, K. Schubert, Investigation of the thermal properties of a micro heat exchanger by 3D fluid dynamics simulation, in: Proceedings of the 4th International Conference on Microreaction Technology, Atlanta, USA, 2000, p. 256.
[12] FLUENT® Version 4.5, FLUENT Inc., Lebanon, New Hampshire, 1999.
[13] J.M. Commenge, L. Falk, J.P. Corriou, M. Matlosz, Microchannel reactors for kinetic measurenent: influence of diffusion and dispersion on experimental accuracy, in: Proceedings of the 5th International Conference on Microreaction Technology, Strasbourg, France, 2001, p. 131.
[14] T. Pignet, L.D. Schmidt, J. Catal. 40 (1975) 212.
[15] D.A. Hickman, L.D. Schmidt, Ind. Eng. Chem. Res. 30 (1991) 50.
[16] N.I. Il'chenko, G.I. Golodets, I.M. Avilova, Theor. Exp. Khim. 11 (1975) 56.
[17] J.M. Commenge, L. Falk, J.P. Corriou, M. Matlosz, Optimal design for flow uniformity in microchannel reactors, in: Proceedings of the 4th International Conference on Microreaction Technology, Atlanta, USA, 2000, p. 23.
[18] J.M. Commenge, L. Falk, J.P. Corriou, M. Matlosz, Am. Inst. Chem. Eng. J. 48 (2002) 345.
[19] E.V. Rebrov, M.H.J.M. de Croon, J.C. Schouten, Development of a cooled microreactor for platinum catalyzed ammonia oxidation, in: Proceedings of the 5th International Conference on Microreaction Technology, Strasbourg, France, 2001, p. 49.
[20] H. Löwe, W. Ehrfeld, Electochim. Acta 44 (1999) 3679.
[21] G. Wießmeier, D. Hönicke, Ind. Eng. Chem. Res. 35 (1996) 4412.
[22] S.J. Gentry, J.G. Firth, A. Jones, J. Chem. Soc., Faraday Trans. 70 (1974) 600.
[23] G. Pecchi, P. Reyes, I. Concha, J.L.G. Fierro, J. Catal. 179 (1998) 309.
[24] R.C. Weast (Ed.), CRC Handbook of Chemistry and Physics, First ed., CRC Press, Boca Raton, FL, 1988.
[25] K.P. Brooks, C.J. Call, M.K. Drost, An integrated microchannel combustor/evaporator with low air toxic emissions, in: Proceedings of the AIChE 1998 Spring National Meeting, New Orleans, LA, USA, 1998.
[26] M.K. Drost, C.J. Call, J.M. Cuta, R.S. Wegeng, J. Microscale Thermophys. Eng. 1 (1997) 321.
[27] O. Görke, P. Pfeifer, K. Schubert, Determination of kinetic data of exothermic reaction in the isothermal microstructure reactor based on the example of catalyzed oxidation of hydrogen, in: Proceedings of the 6th International Conference on Microreaction Technology, New Orleans, LA, USA, 2002, p. 262.
[28] D.H. Kerridge, E.G. Polyakov, Refractory Metals in Molten Salts. Their Chemistry, Electrochemistry and Technology, Kluwer Academic Publishers, Dordrecht, 1998.